Supporting Information: Tunable tunneling magnetoresistance in van der Waals magnetic tunnel junctions with 1*T*-$CrTe_2$ electrodes

Hangyu Zhou,[†,‡,¶] Youguang Zhang,[†] and Weisheng Zhao[*,‡]

†*School of Electronic and Information Engineering, Beihang University, Beijing 100191, China*

‡*School of Integrated Circuit Science and Engineering, MIIT Key Laboratory of Spintronics, Beihang University, Beijing 100191, China*

¶*Shenyuan Honors College, Beihang University, Beijing 100191, China*

E-mail: weisheng.zhao@buaa.edu.cn

Interlayer Binding Energy

We show three different configurations of $CrTe_2$|Gr in Figures S1a-c, marked as Structure 1-3. We also show six different configurations of $CrTe_2$|*h*-BN in Figures S1d-i, marked as Structure 4-9. In order to find the most stable interlayer structure of $CrTe_2$|Gr ($CrTe_2$|*h*-BN),

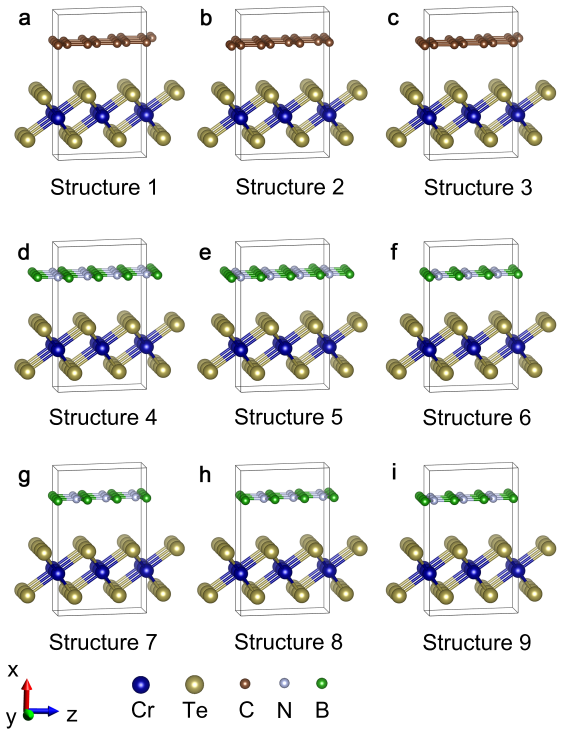

Figure S1: **a-c** The atomic structure of three different configurations of $CrTe_2$|Gr, marked as Structure 1, Structure 2, and Structure 3. **d-i** The atomic structure of six different configurations of $CrTe_2$|*h*-BN, marked as Structure 4, Structure 5, Structure 6, Structure 7, Structure 8, and Structure 9.

we calculated the interlayer binding energy as a function of the separation of the graphene (*h*-BN) sheet from $CrTe_2$. The interlayer spacing between $CrTe_2$ and graphene (*h*-BN) was relaxed considering vdW interaction. The results are shown in Figure S2. One can see that the binding energies of the three $CrTe_2$|Gr structures are almost the same and the most stable interlayer spacing between $CrTe_2$ and graphene is 3.67 Å, as shown in Figure S2a. We choose the interlayer configuration of Structure 1 with a distance of 3.67 Å in our further calculations

for $CrTe_2$|Gr(n ML)|$CrTe_2$ vdW MTJs. However, when comes to the structures formed by $CrTe_2$ and h-BN, the interlayer structure with the Structure 4 configuration, which has the lowest energy with the interlayer spacing of 3.64 Å as shown in Figure S2b, is energetically favorable. Therefore, the interlayer configuration of Structure 4 with a distance of 3.64 Å is chosen in our further calculations for $CrTe_2$|h-BN(n ML)|$CrTe_2$ vdW MTJs. However, through TMR calculations of vdW MTJs with the less stable interlayer configurations, we find that the interface has a very limited effect on the TMR ratio.

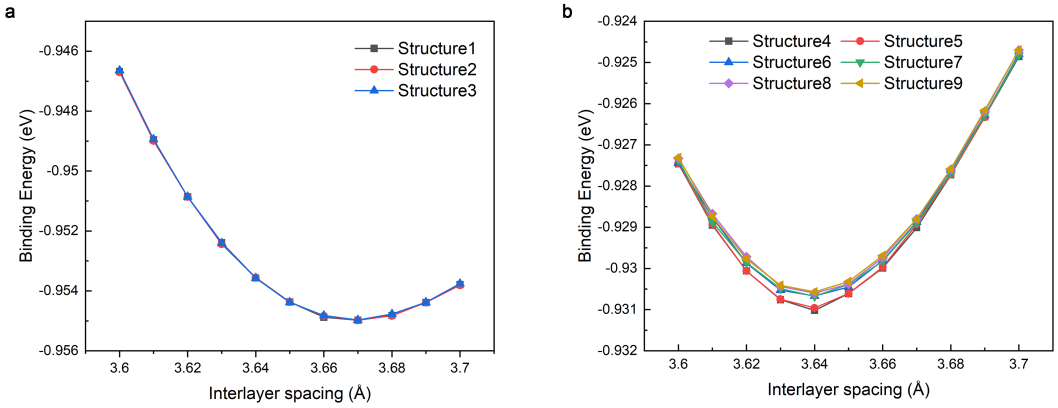

Figure S2: The interlayer binding energy as a function of the separation of the graphene or h-BN sheet from $CrTe_2$. **a** Results of three $CrTe_2$|Gr structures. **b** Results of six $CrTe_2$|h-BN structures.

Schematic diagram of $CrTe_2$|Gr-B(n ML)|$CrTe_2$ vdW MTJ

After the binding energy testing, we built the stable configuration of Gr-B, and schematic diagrams of substitutional doping position in the vdW MTJs with varying layers of graphene are shown in Figure S3.

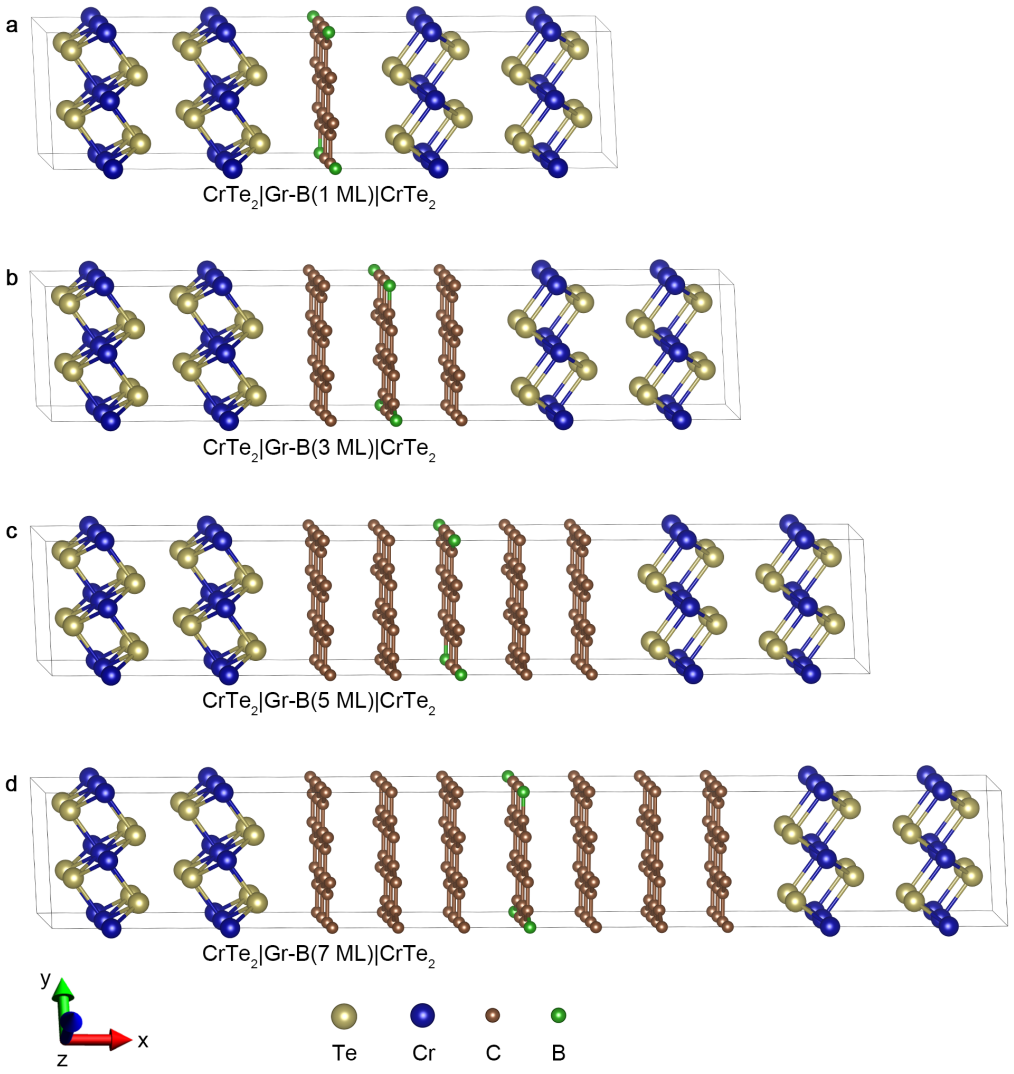

Figure S3: Schematic diagram of $CrTe_2$|Gr-B(n ML)|$CrTe_2$ vdW MTJ.

Transmission spectra and energy-resolved TMR ratio

Here we present the energy-resolved transmission spectra of 1 ML, 3 ML, 5 ML, and 7 ML graphene-barrier junctions in parallel configuration (PC). We also present the transmission spectra after substitutional doping. The results are shown in Figure S4. As expected, we can see that the magnitude of transmission coefficient decreases with the increase of barrier thickness. As shown in Figure S4a-d, $T_{\mathrm{PC}}^{\uparrow}(E)$ is obviously larger than $T_{\mathrm{PC}}^{\downarrow}(E)$ in the energy range of -0.5 to -0.2 eV. The peaks of $T_{\mathrm{PC}}^{\uparrow}(E)$ shift to the Fermi energy (E_{F}) after substitutional doping. Besides, we calculated the energy-resolved TMR ratio of the vdW MTJs before and after substitutional doping by the energy-resolved transmission coefficients, and the results are presented in Figure S5. We can find that the energy-resolved TMR ratio of each vdW MTJ has a peak in the energy range of -0.5 to -0.3 eV. The $CrTe_2$|Gr(7 ML)|$CrTe_2$ vdW MTJ has the maximum peak of $\mathrm{TMR}(E) = 7.8 \times 10^5\%$ among all the vdW MTJs before substitutional doping. After the substitutional doping, we notice that all the peak of $\mathrm{TMR}(E)$ shift to E_{F}, and $\mathrm{TMR}(E)$ peaks of $CrTe_2$|Gr-B(n ML)|$CrTe_2$ vdW MTJs decrease except $CrTe_2$|Gr-B(7 ML)|$CrTe_2$ vdW MTJ. For $CrTe_2$|Gr-B(7 ML)|$CrTe_2$ vdW MTJ, the peak of $\mathrm{TMR}(E)$ increases, reaching $8.5 \times 10^5\%$. By comparing the spectra of $\mathrm{TMR}(E)$, we conclude that the barriers before and after substitutional doping change a lot. MTJs with different barrier materials may have different trends of TMR ratios with increasing barrier thickness,[1] and substitutional doping shifts the Dirac cone of the graphene barrier, which changes the characteristic of graphene. Therefore, we think that it can be hard to judge the trends of TMR ratios with the increase of barrier thickness.

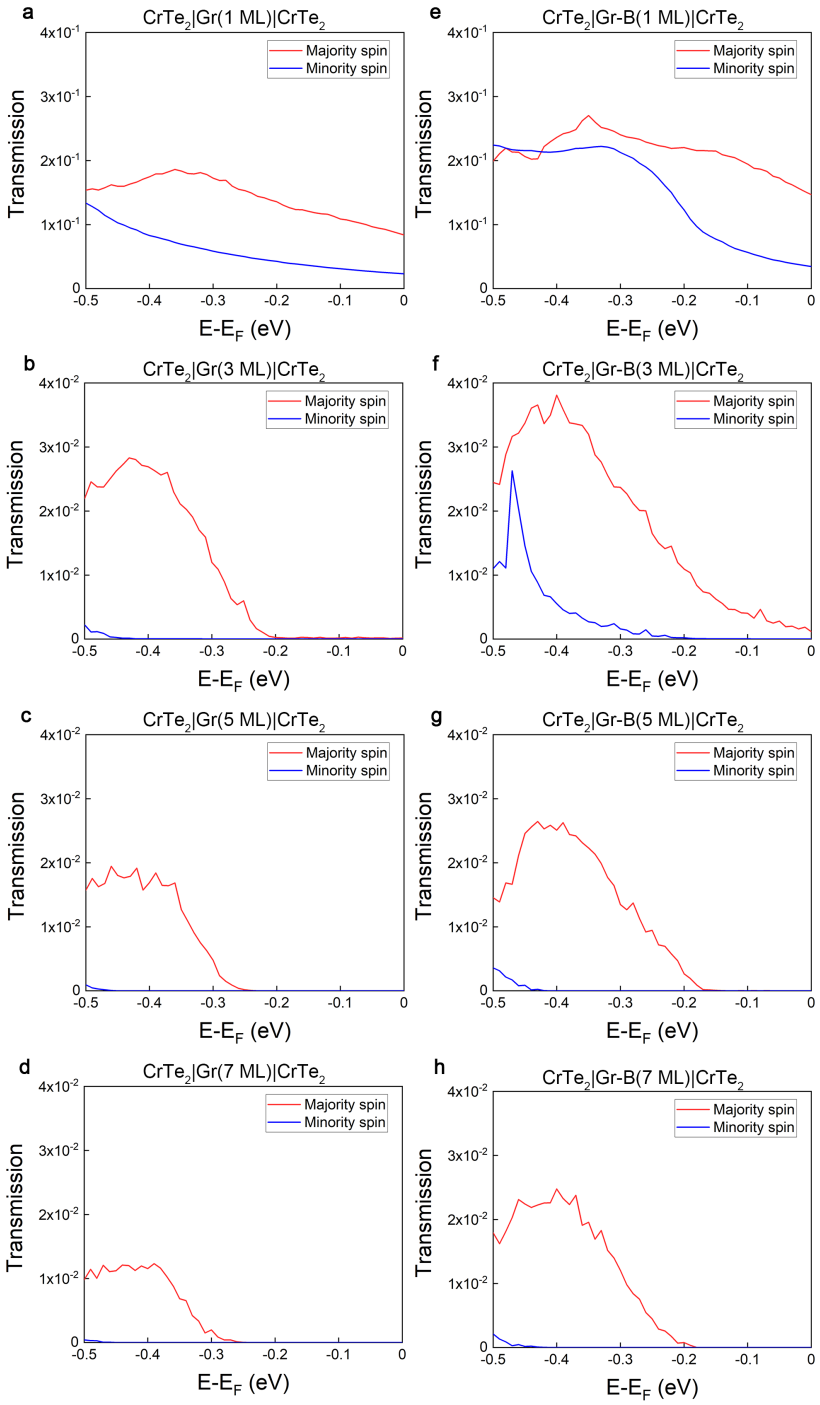

Figure S4: Energy-resolved transmission spectra integrating over all $\mathbf{k}_{\parallel}$ points of varying graphene-thickness vdW MTJs in the parallel configuration (PC). The red color indicates the majority-spin transmission, marked as $T^{\uparrow}_{\mathrm{PC}}(E)$, whereas the blue line indicates the minority-spin transmission, marked as $T^{\downarrow}_{\mathrm{PC}}(E)$. Note that the transmission axis for panel **a** and **e** range from 0 to 4×10^{-1}, whereas that for others ranges from 0 to 4×10^{-2}.

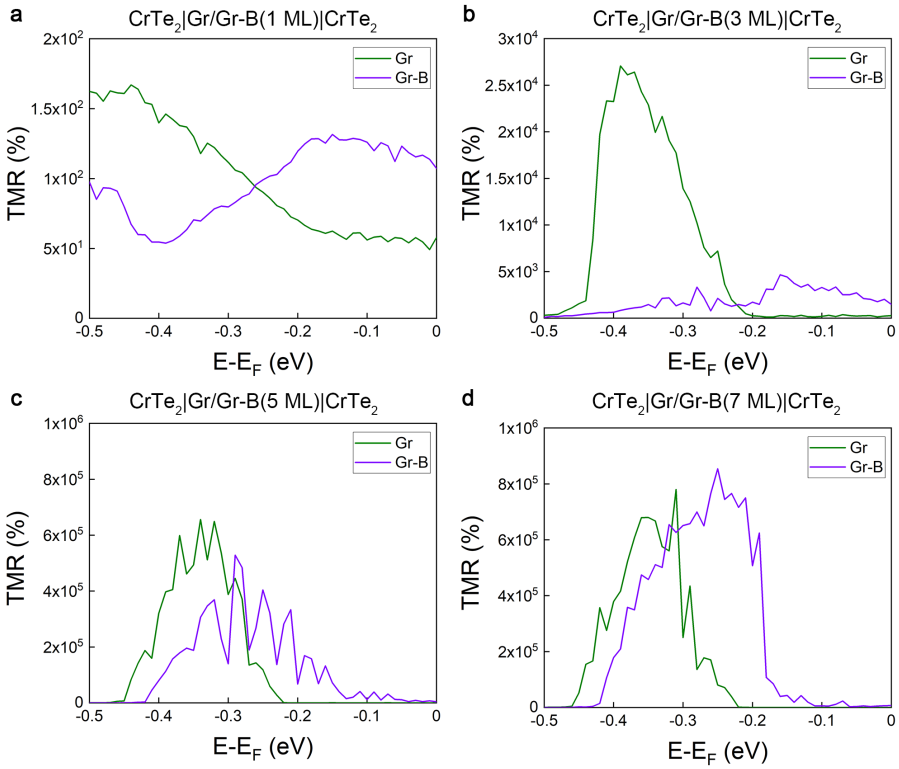

Figure S5: Energy-resolved TMR ratio of varying graphene-thickness vdW MTJs. The energy-resolved TMR ratios were calculated by the energy-resolved transmission coefficients, marked as TMR(E). The green color indicates the TMR ratio of the vdW MTJ with pristine graphene barrier, whereas the purple color indicates the TMR ratio of the vdW MTJ with the B-substituted graphene barrier.

Boron concentration of substitutional doping in graphene barrier

In order to illustrate the relation between boron concentration and the TMR ratio, we substitute two carbon atom with two boron atom in the $CrTe_2$|Gr(3 ML)|$CrTe_2$, $CrTe_2$|Gr(5 ML)|$CrTe_2$, and $CrTe_2$|Gr(7 ML)|$CrTe_2$, abbreviated as $CrTe_2$|Gr-2B(3 ML)|$CrTe_2$, $CrTe_2$|Gr-2B(5 ML)|$CrTe_2$, and $CrTe_2$|Gr-2B(7 ML)|$CrTe_2$. The results are shown in Table S1. Through observing Table S1, we can find that the TMR ratios of 5-ML-barrier junction and 7-ML-barrier junction are enhanced with the increase of the boron concentration. However, when the concentration is too high, the TMR ratio would not be enhanced drastically, such as 482% of $CrTe_2$|Gr-2B (3 ML)|$CrTe_2$ vdW MTJ. Therefore, careful consideration of substitutional doping consideration is needed to enhance the TMR ratio.

Table S1: TMR ratios of vdW MTJs with different boron concentration of substitutional doping in graphene barrier.

	Concentration	TMR ratio
$CrTe_2$|Gr(3 ML)|$CrTe_2$	0	277%
$CrTe_2$|Gr-B(3 ML)|$CrTe_2$	0.019	1478%
$CrTe_2$|Gr-2B(3 ML)|$CrTe_2$	0.037	482%
$CrTe_2$|Gr(5 ML)|$CrTe_2$	0	450%
$CrTe_2$|Gr-B(5 ML)|$CrTe_2$	0.011	4200%
$CrTe_2$|Gr-2B(5 ML)|$CrTe_2$	0.022	4399%
$CrTe_2$|Gr(7 ML)|$CrTe_2$	0	187%
$CrTe_2$|Gr-B(7 ML)|$CrTe_2$	0.0079	6962%
$CrTe_2$|Gr-2B(7 ML)|$CrTe_2$	0.016	13609%

Hubbard Term

$CrTe_2$ is metallic without an energy gap, and the previous studies on $CrTe_2$ neglect the Hubbard term.[2,3] We made a comparison between employing a Hubbard term on the d orbital of Cr and neglecting the Hubbard term by calculating the TMR ratios of the two conditions. The TMR ratio of $CrTe_2$|*h*-BN(n ML)|$CrTe_2$ vdW MTJ, as a representative of

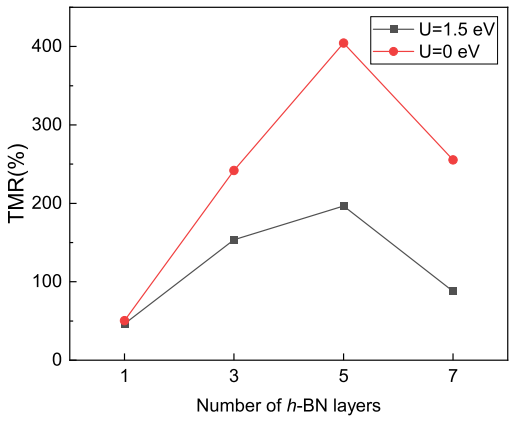

Figure S6: The TMR ratios of $CrTe_2|h$-BN(n ML)$|CrTe_2$ vdW MTJ considering a Hubbard term on the d orbital of Cr with U=1.5 eV and neglecting the Hubbard term.

two types of vdW MTJs, is shown in Figure S6. One can see that the TMR effects of the two conditions show similar trends with varying h-BN layers. We believe that the Hubbard term has no influence on the trend of the TMR ratio. Therefore, for convenient comparison with the previous studies on $CrTe_2$, we neglected the Hubbard term in the present work.

References

(1) Pal, A.; Parto, K.; Agashiwala, K.; Cao, W.; Banerjee, K. Computational Study of Spin Injection in 2D Materials. 2019 IEEE International Electron Devices Meeting (IEDM). 2019; pp 24.2.1–24.2.4.

(2) Lv, H.; Lu, W.; Shao, D.; Liu, Y.; Sun, Y. Strain-Controlled Switch between Ferromagnetism and Antiferromagnetism in 1T-CrX_2 (X= Se, Te) Monolayers. *Phys. Rev. B* **2015**, *92*, 214419.

(3) Freitas, D. C.; Weht, R.; Sulpice, A.; Remenyi, G.; Strobel, P.; Gay, F.; Marcus, J.; Núñez-Regueiro, M. Ferromagnetism in Layered Metastable 1T-$CrTe_2$. *J. Phy.: Condens. Matter* **2015**, *27*, 176002.